Coordination chemistry of manganese and iron with N,O-donor ligands: oxidation catalysis and magnetochemistry of clusters

Godbole, M.D.

2

Highly Efficient Disproportionation of Dihydrogen Peroxide: Synthesis, Structure, and Catalase Activity of Manganese Complexes of the Salicylimidate Ligand*

*Three new manganese complexes namely, $[Mn_2(Etsalim)_4(HEtsalim)_2](ClO_4)_2$ (**1**), $[Mn(Mesalim)_2(OAc)(MeOH)]\bullet MeOH$ (**2**), and $[Mn(Mesalim)_2Cl]$ (**3**) in which HMesalim and HEtsalim are methyl and ethyl salicylimidate, have been synthesized, fully characterized by X-ray analyses, magnetic-susceptibility, UV-Vis and IR spectroscopy, and their catalase activity has been studied. Complex **1** is dinuclear with a Mn–Mn distance of 3.37 Å while the complexes **2** and **3** are mononuclear. All complexes catalyze the disproportionation of dihydrogen peroxide into water and dioxygen; they show very high catalase activity exhibiting saturation kinetics. The rate and turnover numbers of the catalyzed reaction increase dramatically when a few equivalents of base (NaOH) are added to the reaction mixture. The turnover numbers for dihydrogen peroxide disproportionation increase from approximately 200 to more than 1500 in less than 2 minutes per manganese ion for all complexes after addition of few equivalents of NaOH. Kinetic studies of the catalyzed reaction performed on the dinuclear complex **1** in the presence of 5 eq. NaOH, gives k_{cat} = 807 (± 16) s^{-1} and K_M = 0.091 (± 0.003) M. The effective catalytic efficiency is k_{cat}/K_M = 8900 $M^{-1}s^{-1}$. The kinetic parameters of the mononuclear complex **2** in the presence of 5 eq. NaOH, are k_{cat} = 190 (± 4) s^{-1} and K_M = 0.022 (± 0.001) M. The effective catalytic efficiency is k_{cat}/K_M = 8600 $M^{-1}sec^{-1}$. ESI-MS analyses in deuterated solvents have been used to understand the nature of the active species formed on addition of 5 eq of NaOH.*

* This chapter is based on: M.D. Godbole, E. Bouwman, *et al. Inorg. Chim. Acta*, *2004*, *358*, 233-238 and M. D. Godbole, M. Kloskowski, E. Bouwman, *et al. Eur. J. Inorg. Chem.*, 2005, 305- 313

2.1 Introduction

Manganese is present in the active sites of enzymes, such as superoxide dismutase (SOD), manganese catalase, extradiol dioxygenase, arginase and ribonucleotide reductase, the oxygen-evolving complex (OEC) of photosystem II (PS-II), and lipoxygenase.[1] The mechanisms of action of these enzymes are very diverse and include electron transfer (SOD, catalase), the reduction of ribonucleotides to water and deoxyribonucleotides, the oxidation of thiosulfate to sulfate and the four-electron oxidation of water to dioxygen in Photosystem II.[2] The principal mechanism of defense of living cells makes use of superoxide dismutase or catalase enzymes to protect the cell structure against harmful and reactive oxygen species, such as superoxide radicals or dihydrogen peroxide. In addition to widely distributed heme-type catalases, a second class of relatively rare manganese catalases has been found in three bacteria, *Lactobacillus plantarum*,[3] *Thermus thermophilus*,[4] and *Thermoleophilium album*.[5] A dinuclear active site is present in these Mn-catalases, possessing either a Mn^{II}–Mn^{II} or Mn^{III}–Mn^{III} dinuclear complex bridged by a μ-(1,3) carboxylate from glutamate and two μ-oxo bridges from solvent molecules that electronically couple the metal centers. The rate of oxygen evolution by these enzymes is very high, i.e. of the order of 10^5 to 10^6 molecules per second.[6] There is high interest in understanding the chemistry of dinuclear manganese complexes, as much structural and mechanistic information regarding the activity of the enzyme could be obtained through studies on model complexes.[7, 8] The interaction of dihydrogen peroxide and dioxygen with dinuclear manganese complexes has been studied in detail by various groups using several structural as well as functional model complexes.[9-11] Interaction of metal complexes of Schiff-base ligands with dihydrogen peroxide has been a matter of study for long time now for many of these have been shown to be good oxidation catalysts[12] or enzyme mimics.[10, 13, 14]

In this chapter, synthesis, full characterization and catalase activity of three

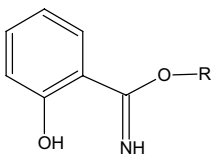

HMesalim, R = CH_3

HEtsalim, R = CH_2-CH_3

Figure 2.1: Schematic drawing of the ligands HMesalim and HEtsalim.

manganese complexes, $[Mn_2(Etsalim)_4(HEtsalim)_2](ClO_4)_2$ (**1**), $[Mn(Mesalim)_2(OAc)(MeOH)]$•MeOH (**2**), and $[Mn(Mesalim)_2Cl]$ (**3**) in which HMesalim and HEtsalim are methyl and ethyl salicylimidate, respectively (shown in Figure 2.1) has been reported. In addition, a comparison of the structural and spectroscopic characteristics of the three complexes is made. The HMesalim ligand is commonly used in organic syntheses as a precursor for several other ligands, such as oxazolines.[15] The transition-metal coordination chemistry of this simple ligand is, however, completely unexplored.

2.2 Experimental Section

2.2.1 Physical Measurements

UV/Vis-NIR measurements were performed on a Perkin-Elmer Lambda 900 UV/Vis/NIR spectrometer. IR spectra were recorded on a Perkin-Elmer FT-IR Paragon 1000 spectrometer. ^{1}H NMR spectra were recorded on a Bruker 300 DPX MHz spectrometer. Elemental analyses were performed with a Perkin-Elmer series II CHNS/O analyzer 2400. EPR measurements were performed at 77 K using a Jeol Esprit RE-2X spectrometer with a Jeol Esprit 330 ESRE data system. EPR *g* values were determined relative to DPPH as an external ''*g*-marker'' (g = 2.0037). Electrospray mass spectra were recorded on a Thermo Finnigan AQA apparatus. All solvents were of analytical grade and used without further purification unless stated otherwise.

2.2.2 Catalase Activity

Two different methods were carried out to obtain the turnover number k_{cat}, the Michaelis constant K_M and k_{cat}/K_M. In the first experiment an aqueous solution of H_2O_2 was added to a solution of the complex at RT. In a typical experiment, to find out the total conversion of dihydrogen peroxide, 2 mmol (2000 eq; 0.17 ml of 35 % aqueous solution) of H_2O_2 was added to 1 ml of a 1 mM solution of the complex in EtOH (for **1**) or MeOH (for **2** and **3**) at RT. Dioxygen evolution was observed instantaneously and monitored manometrically. Initial rate measurements were performed by plotting the volume of dioxygen evolved versus time in seconds.

2.2.3 Kinetic Measurements

For the kinetic studies, an optical dioxygen sensor was used to measure the initial rates of the H_2O_2 decomposition. Therefore the complex was added to an aqueous H_2O_2 solution of increasing concentration and the initial rate was recorded. The data were fit to the Michaelis-Menten equation, and the turnover number (by biochemist's definition) k_{cat}, the

Michaelis constant K_M and k_{cat}/K_M were determined from the double reciprocal Lineweaver-Burk plot (Figure 2.10). K_M is a criterion for substrate affinity, the turnover numb*er* k_{cat} can be interpretated as the rate of substrate conversion to the corresponding products and k_{cat}/K_M is a criterium for catalytic efficiency.

2.2.4 Syntheses.

Caution! Perchlorate salts are potentially explosive and should be handled with appropriate care. The following abbreviations are used throughout the text: HMesalim = Methyl salicylimidate, HEtsalim = Ethyl salicylimidate. All reagents and solvents were used as received with no attempt to remove water or molecular oxygen. The ligand HMesalim was synthesized using the published procedure.[15-17]

$[Mn_2(Etsalim)_4(HEtsalim)_2](ClO_4)_2$ (1): 0.2 g (1.32 mmol) of the ligand HMesalim was dissolved in 10 ml of absolute EtOH. 0.108 g (0.44 mmol) of manganese(II) perchlorate was added to the solution. The solution was stirred for 15 minutes and filtered. Green crystals were obtained after a few days by layering the reaction mixture with ether and hexane. Yield of crude product: 55% (0.156 g) UV-VIS (CH_3CN): λ_{max}/nm (ε/M^{-1} cm^{-1}) = 304 (38 × 103), 357 (20 × 103), 418 (2400), 565 (400), 971 (76); IR (diamond): 3268(m), 1606(s), 1588(s), 1455(s), 1399(s), 1214(m), 1088(vs), 959(m), 868(m), 758(s), 618(s), 523(s), 427(s) cm^{-1}; Elemental analysis calc (%) for **1** ($C_{27}H_{31}ClMnN_{30}O_{10}$, FW = 1295.88): C, 50.05; H, 4.82; N, 6.4. Found: C, 50.0; H, 5.07; N, 6.67; μ_B = 4.8 BM per manganese(III); ESI-MS: 383 $[Mn^{III}(Etsalim)_2]^+$, 429.22 $[Mn^{III}(Etsalim)_2(EtOH)]^+$, 811.35 $[Mn^{III}{}_2(Etsalim)_4(EtOH)–H^+]^+$, 865.30 $[Mn^{III}{}_2(Etsalim)_4(ClO_4)]^+$.

$[Mn(Mesalim)_2(OAc)(MeOH]$•MeOH (2): 1.85 g (12.25 mmol) of the ligand HMesalim was dissolved in 10 ml of absolute MeOH. 1 g (4.08 mmol) of manganese(II) acetate was added to the solution, and the solution was stirred for 15 minutes. Then 20 ml ether was added to the solution, and again the reaction mixture was stirred for 15 minutes. The solution was filtered, and crystals were grown in a few days by layering the MeOH-ether solution with hexane. Yield of the crude product: 61.5% (1.2 g) UV/Vis (CH_3CN): λ_{max}/nm (ε/M^{-1} cm^{-1}) = 304 (16 × 103), 353 (9 × 103), 411 (1860), 562 (277); IR (diamond): 3446(m), 3167(m), 1609(s), 1590(s), 1542(vs), 1452(s), 1412(s), 1330(m), 1231(vs), 1158(s), 1098(s), 863(s), 748(s), 626(s), 492(s) cm^{-1}; Elemental analysis calc (%) for **2**·MeOH ($C_{20}H_{27}MnN_2O_8$·MeOH, FW = 510.42): C, 49.42; H, 6.12; N, 5.49. Found: C, 49.12; H, 6.51; N, 5.86; μ_B= 4.6 BM; ESI-MS: 354.5 $[Mn^{III}(Mesalim_2)]^+$, 415 $[Mn^{III}(Mesalim)_2(OAc) + H^+]^+$, 447 $[Mn^{III}(Mesalim)_2(OAc)(MeOH) + H^+]^+$ and 506 $[Mn^{III}(Mesalim)_3] + H^+]^+$.

[Mn(Mesalim)$_2$Cl] (3): 1 g (6.6 mmol) of the ligand HMesalim was dissolved in 10 ml of methanol. 0.357 g (2.2 mmol) of solid manganese(II) chloride was added to the methanolic solution. The green solution was stirred for about 15 minutes; ether was added to the solution and the reaction mixture was filtered. Green crystals were obtained by slow evaporation of the solution. Yield of crude product: 80% (0.68 g), UV/VIS (CH_3CN): λ_{max}/ nm (ε/M^{-1} cm^{-1}) = 311 (11×10^3), 351 (6230), 421 (1120), 568 (295); IR (diamond): 3263(m), 1615(s), 1590(s), 1455(m), 1393(s), 1215(s), 747(s), 521(s), 411(s) cm^{-1}; Elemental analysis calc (%) for **3** ($C_{16}H_{16}ClN_2MnO_4$, FW= 390.70): C, 49.19; H, 4.13; N, 7.17; Found: C, 48.94; H, 4.08; N, 7.33; μ_B = 4.8 BM; ESI-MS: 354.5 $[Mn^{III}(Mesalim_2)]^+$.

2.2.5 X-ray Crystallographic Study

Intensity data for single crystals of **1**, **2** and **3** were collected at 150 K using graphite-monochromated MoK_α radiation, on a Nonius KappaCCD diffractometer on a rotating anode. A correction for absorption was considered unnecessary in the case of **1** and **3**. For **2**, a multi-scan absorption correction was applied using PLATON/MULABS (0.678-0.903 transmission range).[18] The structures were solved by direct methods using SHELXS97[19] (**1** and **3**) or SIR97[20] (**2**), and refined on F^2 using SHELXL97.[19] All non-hydrogen atoms were refined with anisotropic displacement parameters. All hydrogen atoms, and in particular those attached to nitrogen and oxygen, were positively identified in a difference Fourier map. The position of the hydroxyl hydrogen of the coordinated methanol molecule in **2** was refined with a restraint on the O–H distance. All other hydrogen atoms were constrained to idealized geometries and allowed to ride on their carrier atoms. All hydrogen atoms were refined with an isotropic displacement parameter related to the equivalent displacement parameter of their carrier atoms. The crystal of **3** was twinned by 180˚ rotation about (101); the relative fractional contributions of the two twin components are 0.738(3):0.262. Structure validation and molecular graphics preparation were performed with the PLATON package. [18]

CCDC- 244114 for **1**, 244115 for **2** and 242564 for **3**, contain the supplementary crystallographic data for these structures.

2.3 Results and Discussion

2.3.1 Synthetic Aspects

The ligand HMesalim has been known for over 30 years and is commonly used as a precursor for the synthesis of heterocyclic ligands. Surprisingly, it has very rarely been used in transition metal chemistry. The coordination chemistry of this ligand, however, appears to be very rich.[21-24] Reaction of $Mn(ClO_4)_2$ with HMesalim in ethanol unexpectedly results in the formation of the dinuclear, phenoxo-bridged complex **1**, with the methoxy group on the ligand exchanged with the solvent ethoxy group. ESI-MS analyses of a solution of the ligand HMesalim in ethanol shows two peaks, one for HMesalim and another for HEtsalim, indicating that the presence of a Lewis acid is not necessary for solvolysis to occur. The complex **1** was synthesized by initially dissolving the HMesalim ligand in ethanol, thus, in fact by reaction of the manganese salt with HEtsalim formed *in situ*. The Mesalim-analog of **1** might also be formed in the solution, but complex **1** is the sole product isolated from the

Table 2.1:Crystallographic data for complexes, $[Mn_2(Etsalim)_4(HEtsalim)_2](ClO_4)_2$ (**1**), and $[Mn(Mesalim)_2(OAc)(MeOH)]\cdot MeOH$ (2·MeOH), (**2**) and $[Mn(Mesalim)_2Cl]$ (**3**).

	1	**2**•MeOH	**3**
Formula	$C_{54}H_{62}Cl_2Mn_2N_6O_{20}$	$C_{20}H_{27}MnN_2O_8$	$C_{16}H_{16}ClMnN_2O_4$
Fw, g/mol	1295.88	478.38	390.70
a, Å	10.7886(2)	30.5140(7)	7.289(2)
b, Å	11.7621(2)	30.5140(7)	9.675(2)
c, Å	11.9448(3)	12.3108(4)	12.146(4)
α, deg	105.827(1)	90	84.55(1)
β, deg	92.536(1)	90	77.74(1)
γ, deg	100.032(1)	120	71.08(1)
V, Å^3	1429.24(5)	9926.9(5)	791.4(4)
Z	1	18	2
space group	$P\bar{1}$	$R\bar{3}$	$P\bar{1}$
crystal system	triclinic	rhombohedral	triclinic
ρ_{calc}, g/cm^3	1.506	1.440	1.639
T, K	150	150	150
μ, cm^{-1}	6.17	6.47	10.3
R, *wR*2	0.044, 0.1029	0.0408, 0.109	0.052 (0.121)
S	1.03	1.04	1.18

reaction mixture. When the reaction is performed in methanol a green product is isolated, which has an IR spectrum similar to that of the complex **1**, but crystals good enough for structure determination could not be obtained and the product also did not give good elemental analyses. The synthesis of complex **2** is more complicated. The recrystallization of a concentrated solution of the reaction mixture, by slow evaporation or ether diffusion, gave the complex **2** in pure form. Recrystallization of a dilute solution lead to the formation of several polynuclear manganese clusters over time, thus making the isolation of this pure mononuclear compound difficult. In fact two novel clusters, a hexanuclear cluster with an interesting double-cubane structure, and the other octanuclear cluster have been isolated and crystallographically characterized after attempts at recrystallization of the mononuclear complex **2** as will be discussed in chapter 5 of this thesis.

2.3.2 Description of the Crystal Structures

The X-ray structures of the three new manganese complexes, $[Mn_2(Etsalim)_4(HEtsalim)_2](ClO_4)_2$ (**1**), $[Mn(Mesalim)_2(OAc)(MeOH]$ (**2**) and $[Mn(Mesalim)_2Cl]$ (**3**) have been determined. For all complexes, numerical data and details of the data collection and refinement are presented in Table 2.1 and selected bond distances and angles are given in Table 2.2. A PLUTON projection of the dinuclear complex **1** is shown in Figure 2.2. The molecule is located on an inversion center. Each manganese(III) ion is bound by four different Etsalim ligands, in a distorted octahedral N_2O_4 geometry. Two *trans* chelating ligands, one of which participates in a μ-phenoxo bridge to the other manganese center, form the equatorial plane of the octahedron. One axial site is occupied by the phenolate oxygen atom of a terminally binding ligand and the other by bridging phenolate oxygen from the symmetry-related manganese center. The Mn–O and Mn–N distances are comparable to other Mn(III) complexes of this type that are known in literature.[25] The axial Mn–O(57) an Mn–O(17a) distances are considerably longer (~ 0.2-0.4 Å) than the Mn–O(phenolate) distances in the equatorial plane. Two μ-phenoxo bridges are present in the dinuclear core, separating the two manganese ions at a distance of 3.3705(5) Å. This distance is within the normal range of phenoxo-bridged Mn^{III} complexes.[25]

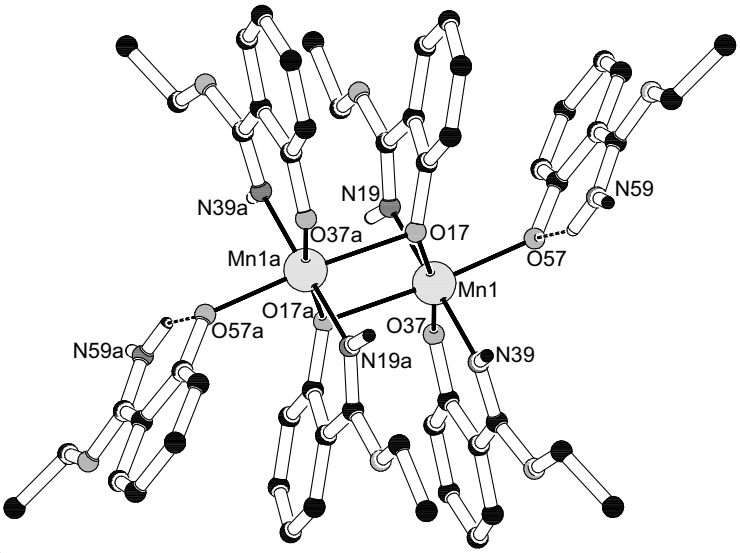

Figure 2.2: PLUTON projection of the complex $[Mn_2(Etsalim)_4(HEtsalim)_2]^{2+}$ cation in complex **1** showing intramolecular hydrogen bonding. Hydrogen atoms, except those attached to the nitrogens, are omitted for clarity.

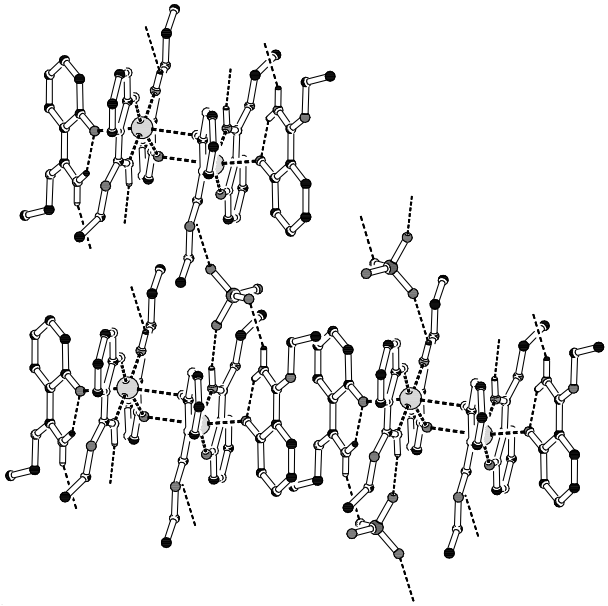

Figure 2.3: A PLUTON projection of packing and hydrogen bonding in the complex **1**.

The Mn(1)–O(17)–Mn(1a) angle of 103.99(6)° is also similar to those in Mn^{III}-salen complexes.[25] Protonation of the imine nitrogens on the two terminal ligands leaves two

Table 2.2: Selected bond distances (Å) and angles (deg) for **1**, **2** and **3**. Symmetry code: a) 1–*x*, –*y*, 2–*z*.

1		**2**		**3**	
Mn(1)–N(19)	1.9927(17)	Mn(1)–N(19)	2.007(2)	Mn(1)–N(19)	1.986(4)
Mn(1)–N(39)	2.0005(18)	Mn(1)–N(39)	2.018(2)	Mn(1)–N(39)	1.991(4)
Mn(1)–O(17)	1.9133(15)	Mn(1)–O(17)	1.8914(17)	Mn(1)–O(17)	1.858(3)
Mn(1)–O(37)	1.8487(15)	Mn(1)–O(37)	1.8850(17)	Mn(1)–O(37)	1.846(3)
Mn(1)–O(57)	2.1284(16)	Mn(1)–O(51)	2.1535(18)	Mn(1)–Cl(1)	2.4220(17)
Mn(1)–O(17a)	2.3507(15)	Mn(1)–O(61)	2.2698(18)	N(19)–Mn(1)–O(17)	90.35(15)
Mn(1)–O(17)–Mn(1a)	103.99(6)	O(17)–Mn(1)–O(37)	88.70(7)	N(19)–Mn(1)–O(37)	86.40(15)
O(17)–Mn(1)–O(37)	168.99(7)	O(17)–Mn(1)–O(51)	95.50(8)	N(39)–Mn(1)–O(17)	87.22(15)
O(17)–Mn(1)–O(57)	90.07(6)	O(17)–Mn(1)–O(61)	87.05(8)	N(39)–Mn(1)–O(37)	90.40(15)
O(17)–Mn(1)–N(19)	87.94(7)	O(17)–Mn(1)–N(19)	89.68(8)	N(19)–Mn(1)–N(39)	163.34(17)
O(17)–Mn(1)–N(39)	94.33(7)	O(17)–Mn(1)–N(39)	174.09(10)	O(37)–Mn(1)–O(17)	160.47(17)
O(37)–Mn(1)–O(57)	100.31(7)	O(37)–Mn(1)–O(51)	91.53(9)	Cl(1)–Mn(1)–O(37)	98.96(12)
O(37)–Mn(1)–N(19)	87.73(7)	O(37)–Mn(1)–O(61)	94.71(9)	Cl(1)–Mn(1)–O(17)	100.56(12)
O(37)–Mn(1)–N(39)	89.97(7)	O(37)–Mn(1)–N(19)	178.12(9)	Cl(1)–Mn(1)–N(19)	98.44(12)
N(19)–Mn(1)–O(57)	93.70(7)	O(37)–Mn(1)–N(39)	88.97(8)	Cl(1)–Mn(1)–N(39)	98.21(13)
N(39)–Mn(1)–O(17a)	90.84(6)	O(51)–Mn(1)–O(61)	173.32(7)		
O(17a)–Mn(1)–O(37)	93.83(6)	O(51)–Mn(1)–N(19)	89.56(9)		
O(57)–Mn(1)–N(19)	93.70(7)				
O(57)–Mn(1)–N(39)	86.65(7)				
O(17a)–Mn(1)–O(57)	165.64(6)				
N(19)–Mn(1)–N(39)	177.70(8)				
O(17a)–Mn(1)–N(19)	89.37(6)				

positive charges on the complex that are balanced by two perchlorate ions present in the crystal lattice. Each of the imine groups is involved in hydrogen bonding with perchlorate ions in the crystal lattice. The free imine group of the terminal ligand participates in an additional intramolecular hydrogen bond with the coordinated phenolate oxygen of the same ligand. (Figure 2.3) The details of the hydrogen bonding interactions are given in Table 2.3.

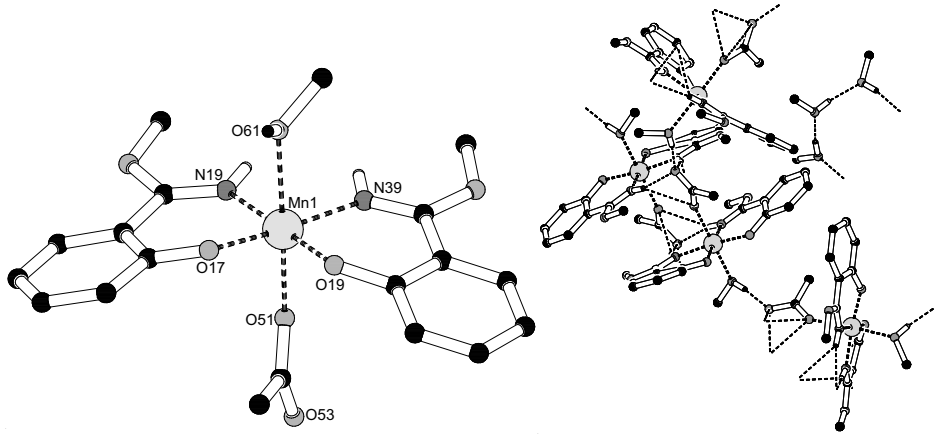

Figure 2.5: A: PLUTON projection of [Mn(Mesalim)$_2$(OAc)(MeOH)] (**2**). Hydrogen atoms except those attached to nitrogens and methanol are omitted for clarity. **B:** PLUTON projection of hydrogen bonding in [Mn(Mesalim)$_2$(OAc)(MeOH)] (**2**)

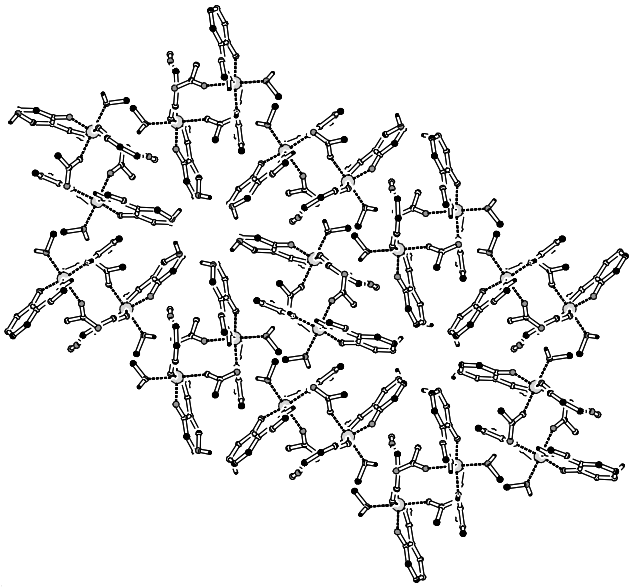

Figure 2.4: Projection of part of the crystal structure of **2** down the [0 0 1] axis. Solvent methanol molecules joined in hydrogen bonded six-membered rings around the threefold screw axes.

A PLUTON projection of the mononuclear complex **2** is shown in Figure 2.5A. The manganese(III) ion has a distorted octahedral N_2O_4 coordination environment. Two chelating Mesalim ligand molecules are bound to the metal, *cis* to each other in the square plane. A methanol and a monodentate acetate molecule occupy the two remaining apical positions and complete the octahedron. The Mn–N and Mn–O distances involving the Mesalim ligand are

slightly longer than those in the complex [Mn(Mesalim)$_2$Cl] (**3**), perhaps due to involvement of the ligands in extensive hydrogen bonding interactions. A PLUTON view of the hydrogen bonding in the crystal lattice is shown in Figure 2.5B, and geometric parameters for the intermolecular hydrogen bonding interactions are listed in Table 2.3. The complex molecules are paired in a head-to-tail arrangement to form a dimer. Both oxygens from the monodentate acetate ion of each complex molecule form bifurcated hydrogen bonds to each of the two cis imine nitrogens on the neighboring complex molecule and vice versa. Thus, the axially coordinated acetate molecule seems to enforce a cis coordination of the Mesalim ligands to allow strong hydrogen bonding. The non-coordinated acetate oxygen atom of each complex molecule forms an additional hydrogen bond to the methanol molecule of a neighboring dinuclear complex and vice versa. The methanol solvent molecule undergoes intermolecular hydrogen bonding with itself, forming a six-membered ring. A view down the [001] direction of 2·MeOH is presented in Figure 2.4. The metal complex cocrystallizes with one more molecule of methanol as observed from the elemental analyses of the complex.

A PLUTON projection of the mononuclear complex **3** is shown in Figure 2.6. Complex **3** crystallizes in the space group P-1. The manganese(III) ion is in a square-pyramidal geometry in an N_2O_2Cl chromophore. Two ligand molecules are bound to the metal, *trans* to each other in the square plane. The chloride ion is coordinated in the apical position at 2.422 Å. The Mn–O and Mn–N distances are typical of Mn(III). There are no hydrogen bonding, or stacking interactions present neither within the molecule nor intermolecular. The lack of interactions is unexpected and quite unusual; a bridging chloride ion would allow the formation of an octahedral geometry. Furthermore several H-bonding interactions would be possible, but none are observed. The analogous complex, [Mn(Mesalim)$_2$(OAc)(MeOH)]•MeOH (**2**) shows the presence of a coordinated methanol molecule at the sixth coordination site on manganese and it shows extensive hydrogen bonding interactions in the crystal lattice as well.

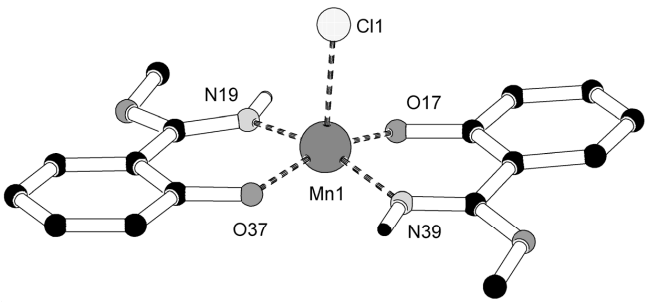

Figure 2.6: PLUTON projection of [Mn(Mesalim)$_2$Cl] (**3**)

Table 2.3: Hydrogen bond details (distances [Å] and angles [º]) for compounds **1** and **2**·MeOH.[a,b] symmetry codes: a) –*x*, –*y*, 1–*z*; b) 1–*x*, –*y*, 1–*z*; c) 1/3–*x*, 2/3–*y*, 2/3–*z*; d) *x*–*y*, *x*, 1–*z*; e) *y*, –*x*+*y*, –*z*.

Donor (D)–H···Acceptor (A)	H···A	D···A	D–H···A
1			
N19– H19···O4a	2.45	3.251(3)	152
N39– H39···O3b	2.28	3.131(3)	162
N59– H59A···O5b	2.15	2.987(3)	159
N59– H59B···O57	1.87	2.567(3)	135
2•MeOH			
N19– H19···O51c	2.57	3.210(3)	130
N19– H19···O53c	2.19	3.044(3)	164
N39– H39···O51c	2.47	3.098(3)	129
N39– H39···O53c	2.28	3.126(3)	162
O61– H61···O53d	1.77(3)	2.616(3)	174(3)
O71– H71···O71e	1.88	2.711(4)	169

(a) D–H distances are all constrained to 0.88 Å except for O61–H61···O53d and O71–H71···O71e that is 0.84 Å.
(b) Symmetry codes : a) –*x*, –*y*, 1–*z*; b) 1–*x*, –*y*, 1–*z*; c) 1/3–*x*, 2/3–*y*, 2/3–*z*; d) *x*–*y*, *x*, 1–*z*; e) *y*, –*x*+*y*, –*z*.

The present complex **3** has the ligands bound to the metal in a *trans* manner, while the complex **2** has the two ligands bound to the metal in a *cis* geometry. The differences in ligand coordination are clearly reflected in the bond distances around manganese in the two complexes. All bonds to the ligand nitrogen and oxygens are longer in complex **2** than in complex **3** due to this difference in ligand geometries and because of the extensive hydrogen bonding interactions in complex **2**. The structure of complex **3** can also be compared to the complex $[Mn(phox)_3]$, which shows weaker bonds to the nitrogens and oxygens as compared to those of complex **3**, i.e. Mn(1)–N(21) = 2.060 and Mn(1)–O(11) = 1.882 Å in the complex $[Mn(phox)_3]$.[26] This indicates very strong bonding interactions between manganese and the ligands in complex **3**.

2.3.3 Spectroscopic Studies

Complexes **1**, **2** and **3** display ligand field bands that are very similar in position. The molar extinction coefficients of **1** are, however, approximately double of those of absorption intensities of the mononuclear complexes **2** and **3** because of the presence of two manganese centers and six ligands. In all complexes the peak at 304 nm is assigned to π-π* transitions within the ligands, because of its high intensity (> 10^4 $M^{-1}cm^{-1}$). The high-intensity band at 357 nm and shoulder at 418 nm can be assigned to the LMCT transition from the phenoxo

oxygen to Mn(III).[27-29] The low-intensity peak at 567 nm (ε ~ 280 $M^{-1}cm^{-1}$ in the mononuclear complexes and ε = 400 $M^{-1}cm^{-1}$ in the dinuclear complex) can be assigned to a d-d transition, as the position of this band is independent of the anions.[27] In addition to these bands complex **1** also shows a weak absorption at 976 nm (ε = 76 $M^{-1}cm^{-1}$). A band similar to this has also been reported for the dinuclear complex, $[Mn_2O(O_2CCH_3)_2(tacn)_2]^{2+}$ which has a band at 990 nm (ε = 28 $M^{-1}cm^{-1}$).[30] This band can be compared to that of manganese catalase from *Thermus Thermophilus* also, where a broad tail is observed going into the near-IR region and a d-d transition is centered at approximately 492 nm.[31]

The IR spectrum of the free ligand displays a broad peak at 2538 cm^{-1} characteristic of the phenol O–H. The imine C=N frequency in the free ligand occurs at 1653 cm^{-1} and shifts to 1615-1605 cm^{-1} after complexation to Mn in all complexes. The presence of the perchlorate anion in the complex **1** is confirmed by a very intense band at 1088 cm^{-1}. For all complexes N–H stretching vibrations are seen at 3278 cm^{-1} and 3175 cm^{-1}, respectively. For complex **2**, the acetate vibrating modes could not be exactly assigned due to the presence of several ligand peaks in the acetate region.

Room temperature magnetic measurements for all complexes are consistent with the presence of Mn(III). Variable temperature magnetic susceptibility measurements were performed for complex **1**, and a plot of the effective magnetic moment versus temperature is shown in Figure 2.7. The steep decrease in magnetic moment at temperatures below 25 K is due to the zero field splitting typical for Mn(III) ions.

2.3.4 Catalase Activity and Kinetics

The catalase activity of the three complexes $[Mn_2(Etsalim)_4(HEtsalim)_2](ClO_4)_2$ (**1**),

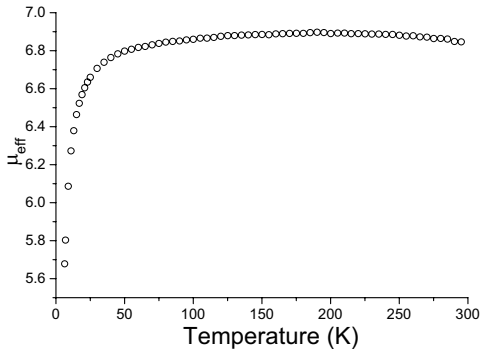

Figure 2.7: Variable temperature magnetic susceptibility of complex **1**.

[Mn(Mesalim)$_2$(OAc)(MeOH)]·MeOH (**2**·MeOH) and [Mn(Mesalim)$_2$Cl] (**3**) has been studied, both in the presence and absence of different amounts of sodium hydroxide (NaOH), because the enhancing effect of small amounts of NaOH on catalase activity has been reported recently.[32]

Addition of dihydrogen peroxide to alcoholic solutions of the new manganese-Mesalim and Etsalim complexes leads to vigorous evolution of dioxygen. The green solutions of the complexes turn brown when NaOH is added, and when subsequently H_2O_2 is added to these alkaline solutions, the reaction mixture turns from brown to colorless, with a brown precipitate, meanwhile showing even more vigorous evolution of dioxygen. The total conversion of dihydrogen peroxide disproportionation was measured using a manometric method while the kinetic studies were performed on the basis of fluorescence quenching using an oxygen sensor.[11, 33] The total catalytic activity as well as the rate of the reaction increases significantly when a few equivalents of NaOH are added. In Table 2.4 the turnover numbers for the disproportionation of H_2O_2 by the manganese complexes in the presence and absence of NaOH are compared. It is interesting to note that the mononuclear complexes **2** and **3** also show very high catalase activity and reach comparable turnovers of manganese ion per minute (TON= ~ 1500), as the dinuclear complex. In fact, the mononuclear complex **2** shows even higher turnovers per manganese ion (1800) than the dinuclear complex **1** (1575). The complexes **2** and **3** show very similar catalase activity possibly indicating that a similar active species is formed.

A plot of the percentage conversion of dihydrogen peroxide for complex **1** followed in time as a function of the amount of NaOH that is added is shown in Figure 2.8. The highest initial rate is observed when 5 equivalents of NaOH are added. When 7 equivalents of NaOH are added, the initial rate is lower than for 5 equivalents of NaOH, but the catalyst is active for a longer time, which results in turnover numbers above 3000 for complex **1** + 5 eq NaOH in less than 2 minutes. A similar observation of a breakpoint in the rate acceleration at 5 eq NaOH addition has been reported previously.[32] When more dihydrogen peroxide is added at the end of a reaction, only very slow evolution of dioxygen occurs, indicating that the catalyst has decomposed. The reactions reach completion within the first two minutes. No lag phase is observed for the reaction with or without addition of NaOH. The blank reaction performed with Mn(II) perchlorate yields only 190 turnovers numbers in total after 4 minutes only in the presence of as much as 5-6 eq. NaOH, while no reaction is observed in the absence of NaOH.

Table 2.4: Disproportionation of dihydrogen peroxide by the three Mn-Mesalim complexes.[a]

Complexes	TON in H_2O_2 (without NaOH)	TON in H_2O_2 (5eq NaOH)	Conversion(%) (5 eq NaOH)
$Mn(ClO_4)_2$	0[b]	190[b]	48%
$[Mn_2(Etsalim)_4(HEtsalim)_2](ClO_4)_2]$ (**1**)	180	3150[c]	90%
$[Mn(Mesalim)_2(OAc)(MeOH)]\cdot MeOH$ (**2**)	350	1810	91%
$[Mn(Mesalim)_2Cl]$ (**3**)	270	1360	68%

a: Reaction conditions: 1 ml of 1 mM solution of the catalyst in methanol (**2**) or ethanol (**1**), H_2O_2 = 2 mmol, RT, turnovers after 3 minutes. (catalyst:H_2O_2 = 1:2000)
b: 5 ml 1 mM catalyst solution used, (catalyst:H_2O_2 = 1:400)
c: 3.5 mmol of H_2O_2 used, (catalyst:H_2O_2 = 1:3500)
TON = Turnover number (moles of substrate molecules converted per mol of the catalyst)

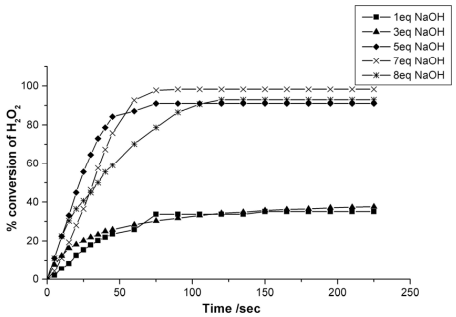

Figure 2.8: Conversion of H_2O_2 in time vs equivalents of NaOH added. Catalyst = $[Mn_2(Etsalim)_4(HEtsalim)_2](ClO_4)_2$ (**1**), Catalyst= 1 μmol and H_2O_2 = 3.18 mmol in 1 ml EtOH.

The kinetics for the catalase reaction of the two complexes **1** and **2** has been studied. Figure 2.9 shows saturation kinetics for the two complexes **1** (Figure 2.9A) and **2** (Figure 2.9B) in combination with 5 eq NaOH each. Figure 2.10 shows Lineweaver-Burk plots of the two systems, demonstrating a linear relationship between the rate of substrate disproportionation and substrate concentration for both systems, from which the Michaelis-Menten parameters can be extracted.

For complex **1** + 5 eq NaOH system, it gives values as k_{cat} = 807 sec^{-1} (± 16) and K_M = 0.091 M (± 0.003) and k_{cat}/K_M = 8900 $M^{-1}sec^{-1}$ (Figure 2.10A) and for complex **2** + 5 eq NaOH system, it gives values as k_{cat} = 190 sec^{-1} (± 4), K_M = 0.022 M (± 0.001) and k_{cat}/K_M = 8600 $M^{-1}sec^{-1}$ (Figure 2.10B). A comparison of the kinetic parameters for the two systems **1** + 5 eq NaOH and **2** + 5 eq NaOH shows that, in fact both of them show similar catalytic efficiency. The value of k_{cat}, the turnover efficiency of the **2** + 5 eq NaOH system, is actually

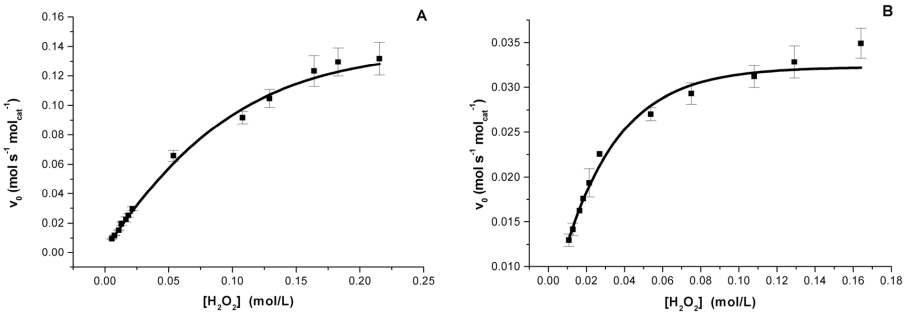

Figure 2.9: (**A**) Initial rate of substrate conversion versus substrate concentration at constant concentration of $[Mn_2(Etsalim)_4(HEtsalim)_2](ClO_4)_2$ (**1**) +5 eq NaOH in ethanol and (**B**) $[Mn(Mesalim)_2(OAc)(MeOH)]$ (**2**) +5 eq NaOH in methanol.

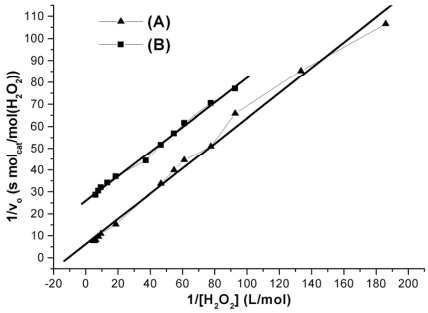

Figure 2.10: Lineweaver-Burk plot for (a) $[Mn_2(Etsalim)_4(HEtsalim)_2](ClO_4)_2$ (**1**) + 5 eq NaOH in ethanol, and (b) $[Mn(mesalim)_2(MeOH)(OAc)]$ (**2**) +5 eq NaOH in methanol

lower than the complex **1** + 5 eq NaOH system, but this is compensated by the very low K_M value. Thus, the ratio k_{cat}/K_M becomes similar to that of complex **1** + 5 eq NaOH. Apparently, the two complexes catalyze the reactions probably by different mechanisms, but ultimately reach similar catalytic efficiency. The nature of the mechanisms however, cannot be anticipated at the moment. The complexes themselves, without addition of NaOH, also show good catalase activity (Table 2.4), but their Michaelis-Menten parameters could not be determined as they did not give saturation kinetics for the range of dihydrogen peroxide concentrations studied.

2.3.5 Spectroscopic Studies on the Catalyst Solution

Ligand field spectra of the complex **1** taken during stepwise addition of NaOH show small, but clear changes with three distinct isobestic points at 310, 350 and 392 nm (Figure 2.11). On addition of 1 and 2 eq NaOH, hardly any changes are observed in the spectrum of the complex **1**. On addition of successive equivalents of NaOH (3 to 10 eq), the peak at 330 starts growing in intensity and the peaks at 357, 418 and 565 nm show a decrease in intensity.

At 5 eq NaOH added, the same trend continues, and no clearly defined new peaks are formed. On addition of higher equivalents of NaOH the peak at 330 nm is of high intensity [27-29] and the spectrum from 400 to 700 nm appears as a broad tail going into the visible region. A brown precipitate appears concomitantly in the solution, indicating degradation of the complex.

A frozen-solution EPR spectrum of a reaction mixture containing only complex **1** and dihydrogen peroxide in ethanol taken 3 minutes after the addition of dihydrogen peroxide (i.e after the reaction has finished) shows a six-line signal typical of Mn(II) (g = 2.01, A = 90 G). No EPR signal can be detected however, after the stepwise addition of NaOH to a solution of **1**, nor after the subsequent addition of dihydrogen peroxide, suggesting that manganese(II), or mixed-valent manganese(III)/(IV) species are not formed in this case.

Positive mode ESI-MS analysis was used to understand the nature of the species formed on addition of NaOH to a solution containing complex **1**. To assist the assignments of peaks the spectra were also measured from the solution of the complex prepared in ethanol-d_6 (C_2D_5OD), as the solvent for elution undeuterated ethanol was used. A part of the complex ions undergo exchange with the deuterated ethanol and due to this a pattern of lines with species ranging from undeuterated, partly deuterated to completely deuterated complex ions can be observed. Analyzing the pattern of peaks, it is clear that the ethoxy group on the ligand is rather labile, and in the metal complex rapidly exchanges with that of the solvent ethanol, consistent with the earlier observation during complex synthesis (see above). Tables listing full details, relative intensities and assignments are given in Appendix A1; Table 1 and Table 2. A solution of complex **1** in ethanol exhibits peaks at 383.15 $[Mn^{III}(Etsalim)_2]^+$, 429.22 $[Mn^{III}(Etsalim)_2(EtOH)]^+$, 811.35 $[Mn^{III}{}_2(Etsalim)_4(EtOH)–H^+]^+$ and 865.30 $\{[Mn^{III}{}_2(Etsalim)_4](ClO_4)\}^+$. The presence of latter two peaks suggests that the dinuclear core of the complex does persist in the solution.

In deuterated ethanol the complex shows clusters of peaks at 383.15 $[Mn^{III}(Etsalim)_2]^+$, 388.19 $[Mn^{III}(Etsalim)(d_5\text{-}Etsalim)]^+$ and 393.19 $[Mn^{III}(d_5\text{-}Etsalim)_2]^+$ and at 429.23 $[Mn^{III}(Etsalim)_2(EtOH)]^+$, 434.26 $[Mn^{III}(Etsalim)(d_5\text{-}Etsalim)(EtOH)]^+$ and 439.29 $[Mn^{III}(d_5\text{-}Etsalim)_2(EtOH)]^+$, as well as 5-line patterns for the dinuclear species in the ranges 811-831 and 865-885. ESI-MS spectra of complex **1** + 5 eq NaOH in ethanol reveal peaks at 451.26 $\{Na[Mn(Etsalim)_3(EtOH)–H^+]\}^+$, 497.28 $\{Na[Mn(Etsalim)_2(EtOH)_2–H^+]\}^+$, 570.35 $\{Na[Mn(Etsalim)_3]\}^+$, 787.47 $\{Na[Mn_2(Etsalim)_4–2H^+]\}^+$, 833.46 $\{Na[Mn_2(Etsalim)_4(EtOH)–H^+]\}$, 850.57 $\{Na[Mn_2(Etsalim)_4(EtOH)(O)]\}^+$, and

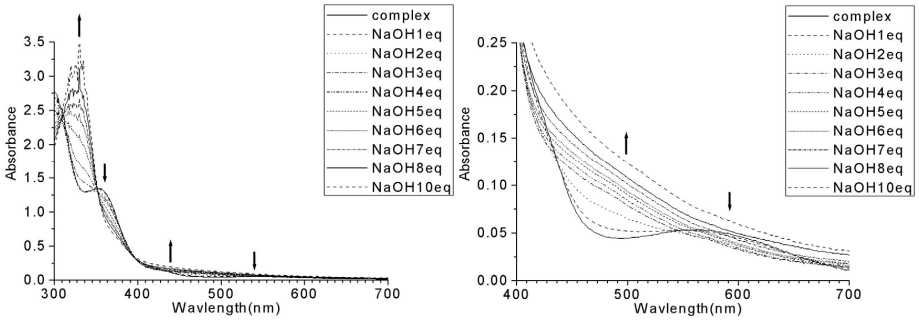

Figure 2.11: Changes in Ligand field spectra to the solution of complex **1** on successive additions of NaOH.

952.57 $\{Na[Mn_2(Etsalim)_5–H^+]\}^+$. The most interesting observation after addition of NaOH is the peak at 850.57, which is tentatively assigned to a dinuclear Mn-μ-oxo species.

These assignments were all confirmed by the presence of the respective multi-line signals in the ESI-MS spectra using deuterated ethanol and NaOH in D_2O. Furthermore, in the deuterated solvent a group of peaks of low intensity at 959-974 is observed, which could possibly be assigned to a di-μ-oxo species, $\{Na^+[Mn^{IV}_2(Etsalim)_4(EtOH)_3(O)_2]\}^+$. However, this species was not observed in undeuterated ethanol which unfortunately makes unambiguous assignment of these peaks not possible. Addition of dihydrogen peroxide to this reaction mixture does not give rise any other peaks in the ESI-MS spectrum, as most of it is degraded before the active species could be measured.

2.3.6 Discussion and Comparison to Other Systems

The k_{cat} and K_M values for the complexes **1** and **2** in combination with 5 eq NaOH, can be compared to those of $[Mn(bpia)(\mu\text{-}OAc)]_2(ClO_4)_2$ (bpia = bis(pyridylmethyl)(N-methylimidazol-2-ylmethyl)amine) which are k_{cat} = 1100 s^{-1}, K_M = 31.5 mM and k_{cat}/K_M = 34000 $M^{-1}s^{-1}$.[11] The present complex **1** or **2** + 5 eq NaOH systems show the second best activity that has been reported till now for the manganese catalase mimics with the Mn(bpia) system in the first position.

For the present studies, addition of few equivalents of base was used successfully for increasing the catalase activity, as has been already reported for other systems.[32] The rate acceleration on addition of NaOH, possibly correlates with the availability of an intramolecular hydroxide for substrate deprotonation and with binding of the substrate at the bridging site between Mn ions in the reductive O–O bond cleavage step.[32] After addition of NaOH, there might be μ-oxo or μ-hydroxo bond formation between the two manganese ions

as is demonstrated by the use of sodium hydroxide for the syntheses of several μ-oxo bridged, dinuclear manganese complexes.[34]

For the $[Mn(2\text{-}OH\text{-}salpn)]_2$ (k_{cat} = 4-22 sec^{-1}) and $[Mn_2(salpn)O_2]$ (k_{cat} = 2500 sec^{-1}) systems (salpn = *N*,*N*′-bis(salicylidene)-1,3-diaminopropane and 2-OH-salpn = N,N'-bis(salicylidene)-(2-hydroxy)-1,3-diaminopropane), the rate increases tremendously when the alkoxo bridged dinuclear complex is replaced by a dinuclear μ-oxo bridged manganese complex.[10] NaOH and N-methyl imidazole were studied as bases in the catalase reaction with the manganese-Mesalim and -Etsalim complexes. Both bases increased the total conversion as well as rate of the catalase reaction. The present system also gives higher catalytic efficiency than the recently reported $[Mn_2(L)_2Cl_2]$ system, (L = 2-{bis(pyridine-2-ylmethyl)aminomethyl}-6-methoxyphenol).[33] The ligand field spectra recorded upon successive additions of NaOH show that the LMCT bands (300 nm and 360 nm) show clear changes with isobestic points indicating formation of one species from the original complex. Addition of more than 5 eq NaOH results in formation of a precipitate, and the ligand field spectrum becomes broadened. ESI-MS analysis proved to be a useful tool for the interpretation of the species formed on addition of NaOH to the complex solution. The first role of NaOH may be to withdraw the proton on the imine nitrogen and thus make the complex more oxidizable. The removal of the proton from the imine nitrogen is evident from the peaks at 787.14, $\{Na^+[Mn_2(L)_4–2H^+]\}^+$ and at 833.18, $\{Na^+[Mn_2(L)_4(EtOH)–2H^+]\}$ on addition of 5 eq NaOH to the complex **1** solution, where both or at least one proton has to be withdrawn from the imine nitrogen on the Etsalim ligand. The only species that could give a hint to the μ-oxo species formation was observed by the peak at 850.57, which could be assigned to a μ-oxo-bridged species with a relative intensity of 10%. Dinuclear Mn(III)/Mn(III) species have been proposed to be the active catalysts for H_2O_2 disproportionation in several manganese catalases as well as functional catalase model complexes. X-band EPR spectra recorded at 77 K did not show signals characteristic for the formation of a Mn(IV) species, or a mixed-valent Mn(II)/Mn(III) or Mn(III)/Mn(IV) species, neither after addition of NaOH nor immediately after addition of dihydrogen peroxide (i.e during catalytic turnover). A brown precipitate that is insoluble in many solvents, characteristic of MnO_2, is formed at the end of the reaction. Thus, the catalytically inactive species formed at the end of the reaction is likely due to the decomposition of the metal complex to form insoluble Mn(IV) oxides.

2.4 Concluding Remarks

In this study the synthesis, crystal structures, full characterization and catalase studies of three manganese complexes have been presented. It has been shown that complexes **1-3** in combination with 5 equivalents of NaOH show very high catalase activity and are only surpassed by the Mn-bpia system reported by Krebs and co-workers.[11] However, compared to the Mn-catalase enzyme, the k_{cat} is still 20-30 times lower than the manganese-catalase enzymes and thus the catalytic efficiency (k_{cat}/K_M) is still 200-300 times lower than that of the manganese-catalase enzymes. The turnovers as well as the rate of the reaction increases remarkably with the addition of a few equivalents of NaOH to the catalyst solution. The complexes in combination with few equivalents of sodium hydroxide (NaOH) are among the few catalase model systems that show turnover numbers up to 3000 in dihydrogen peroxide disproportionation. ESI-MS analyses in deuterated solvents have been used to understand the nature of the active species formed on addition of 5 eq of NaOH. The exact nature of the active species participating during turnover however, could not yet be confirmed.

2.5 References

1. Reedijk, J.; Bouwman, E., in *Bioinorganic catalysis*, Reedijk, J.; Bouwman, E. Ed; Second edition, Marcel Dekker; Inc, New York, 1999.
2. Dismukes, G. C., in *Bioinorganic catalysis*, Reedijk, J. Ed; First Edition, Marcel Dekker, New york, 1993; pp 317-346.
3. Kono, Y.; Fridovich, I., *J. Biol. Chem.* 1983, 258, 3646-3648.
4. Michaud-Soret, I.; Jacquamet, L.; Debaecker-Petit, N.; Le Pape, L.; Barynin, V. V.; Latour, J. M., *Inorg. Chem.* 1998, 37, 3874-3876.
5. Allgood, G. S.; Perry, J. J., *J. Bacteriol.* 1986, 168, 563-567.
6. Penner-Hahn, J., in *Manganese Redox Enzymes*, Pecoraro, V. L. Ed; VCH Publishers, New york, 1992; pp 29-45.
7. Dubois, L.; Caspar, F.; Jacquamet, L.; Petit, P. E.; Charlot, M. F.; Baffert, C.; Collomb, M. N.; Deronzier, A.; Latour, J. M., *Inorg. Chem.* 2003, 42, 4817-4827.
8. Pessiki, P. J.; Dismukes, G. C., *J. Am. Chem. Soc.* 1994, 116, 898-903.
9. Dubois, L.; Xiang, D. F.; Tan, X. S.; Pecaut, J.; Jones, P.; Baudron, S.; Le Pape, L.; Latour, J. M.; Baffert, C.; Chardon-Noblat, S.; Collomb, M. N.; Deronzier, A., *Inorg. Chem.* 2003, 42, 750-760.
10. Gelasco, A.; Bensiek, S.; Pecoraro, V. L., *Inorg. Chem.* 1998, 37, 3301-3309.
11. Triller, M. U.; Hsieh, W. Y.; Pecoraro, V. L.; Rompel, A.; Krebs, B., *Inorg. Chem.* 2002, 41, 5544-5554.
12. Katsuki, T., *Coord. Chem. Rev.* 1995, 140, 189-214.
13. Gelasco, A.; Askenas, A.; Pecoraro, V. L., *Inorg. Chem.* 1996, 35, 1419-1420.
14. Gelasco, A.; Pecoraro, V. L., *J. Am. Chem. Soc.* 1993, 115, 7928-7929.
15. Black, D. S. C.; Wade, M. J., *Aust. J. Chem.* 1972, 25, 1797-1810.
16. Stoss, P., *Chem. Ber.* 1978, 111, 314-319.
17. Vinkler, P.; Thimm, K.; Vob, J., *Liebigs Ann. Chem.* 1976, 1976, 2083- 2093.
18. Spek, A. L., *J. Appl. Crystallogr.* 2003, 36, 7-13.
19. Sheldrick, G. M. *SHELXS-97 and SHELXL-97*, University of Göttingen: Göttingen (Germany), 1997.
20. Altomare, A.; Burla, M. C.; Camalli, M.; Cascarano, G. L.; Giacovazzo, C.; Guagliardi, A.; Moliterni, A. G. G.; Polidori, G.; Spagna, R., *J. Appl. Crystallogr.* 1999, 32, 115-119.

21. Godbole, M. D.; Grigiotti, E.; Zanello, P.; Mills, A. M.; Spek, A. L.; Bouwman, E., *Inorg. Chim. Acta* 2005, 358, 233-238.
22. Godbole, M. D.; Kloskowski, M.; Hage, R.; Rompel, A.; Mills, A. M.; Spek, A. L.; Bouwman, E., *Eur. J. Inorg. Chem.* 2005, 305-313.
23. Godbole, M. D.; Roubeau, O.; Clerac, R.; Kooijman, H.; Spek, A. L.; Bouwman, E., *Chem. Commun.* 2005, 3715-3717.
24. Godbole, M. D.; Roubeau, O.; Clerac, R.; Kooijman, H.; Spek, A. L.; Bouwman, E., *manuscript in preparation*.
25. Shyu, H. L.; Wei, H. H.; Wang, Y., *Inorg. Chim. Acta* 1999, 290, 8-13.
26. Hoogenraad, M.; Ramkisoensing, K.; Kooijman, H.; Spek, A. L.; Bouwman, E.; Haasnoot, J. G.; Reedijk, J., *Inorg. Chim. Acta* 1998, 279, 217-220.
27. Boucher, L. J.; Day, V. W., *Inorg. Chem.* 1977, 16, 1360-1367.
28. Marappan, M.; Narayanan, V.; Kandaswamy, M., *J. Chem. Soc.-Dalton Trans.* 1998, 3405-3409.
29. Neves, A.; Erthal, S. M. D.; Vencato, I.; Ceccato, A. S.; Mascarenhas, Y. P.; Nascimento, O. R.; Horner, M.; Batista, A. A., *Inorg. Chem.* 1992, 31, 4749-4755.
30. Wieghardt, K.; Bossek, U.; Ventur, D.; Weiss, J., *J. Chem. Soc.-Chem. Commun.* 1985, 347-349.
31. Whittaker, M. M.; Barynin, V. V.; Antonyuk, S. V.; Whittaker, J., *Biochemistry* 1999, 38, 9126-9136.
32. Boelrijk, A. E. M.; Dismukes, G. C., *Inorg. Chem.* 2000, 39, 3020-3028.
33. Reddig, N.; Pursche, D.; Kloskowski, M.; Slinn, C.; Baldeau, S. M.; Rompel, A., *Eur. J. Inorg. Chem.* 2004, 879-887.
34. Maneiro, M.; Bermejo, M. R.; Fondo, R.; Gonzalez, A. M.; Sanmartin, J.; Garcia-Monteagudo, J. C.; Pritchard, R. G.; Tyryshkin, A. M., *Polyhedron* 2001, 20, 711-719.